Listening with Light: Acoustic sensing over live fibre networks using Coherent Optical Transceivers

Max Brenner, Alice V Drozdov, and Mitchell A Cox*

School of Electrical and Information Engineering, University of the Witwatersrand, Johannesburg, South Africa

E-mail: Mitchell.Cox@wits.ac.za

Abstract. Environmental vibrations change the state of polarisation and phase of light in optical fibres. Modern coherent transceivers actively track and compensate these distortions using digital signal processing, presenting an opportunity to repurpose this tracked data for environmental sensing purposes. Although polarisation and phase data have enabled sub-Hz geophysical monitoring, their use for audible-frequency acoustic sensing remains unexplored. This paper presents preliminary laboratory results in which airborne sounds interacting with a fibre segment yield clear signatures in both the state of polarisation and carrier-phase data extracted from an optical coherent transceiver, allowing the reconstruction of single tones, frequency sweeps and complex audio. These findings demonstrate proof of concept for acoustic sensing over live fibre links. Future work will quantify the system's sensitivity, bandwidth and noise floor, and investigate sensor-fusion strategies to enhance detection performance.

1 Introduction

Optical fibre infrastructure forms the backbone of modern telecommunications networks [1]. These fibres are sensitive to environmental disturbances like changes in temperature, pressure and vibration, all of which alter the fibre's physical properties and, in turn, modulate the properties of the light within [1]. This inherent sensitivity has been exploited in applications such as earthquake and tsunami sensing [2]. In the field of fibre acoustic sensing, techniques such as Distributed Acoustic Sensing (DAS) are well established but typically require specialist hardware and dedicated dark fibres, precluding deployment on active data-carrying links [3]. Similarly, interferometric methods demand additional costly hardware [3]. An alternative approach makes use of the digital signal processing (DSP) capabilities of modern coherent optical transceivers, which continually estimate channel state information such as the light's state of polarisation (SOP) and carrier phase, to compensate for impairments and recover transmitted data [4]. By analysing this readily available information, recent work has successfully demonstrated the sensing of very low-frequency geophysical phenomena, such as earthquakes and ocean swells, over live transoceanic links [2]. However, the extension of this technique to detect and characterise signals within the human audible acoustic spectrum (20 Hz to 20 kHz [5]) remains largely unexplored. This gap presents an opportunity to repurpose existing live optical fibres for acoustic sensing without incurring the cost of new deployments and while maintaining simultaneous data transmission. This paper presents a preliminary experimental demonstration of audible-range acoustic sensing over a coherent optical link. Single-frequency tones, frequency sweeps and complex broadband audio signals are recovered from both SOP and phase channels extracted from a commercial coherent transceiver. These results demonstrate proof of concept for this method of audible-range acoustic sensing and lay the groundwork for future work, which will focus on comprehensive system characterisation, comparative analysis of SOP and phase sensing channels, as well as sensor fusion techniques to improve signal detection.

2 Sensing Principle and Data Extraction

2.1 Acoustic Modulation of Optical Signals

The principle behind this sensing technique lies in the physical interaction between acoustic waves and the optical fibre. An acoustic wave impinging on a fibre induces time-varying mechanical strain and pressure. These perturbations modulate the properties of the light propagating within, with two properties that are actively tracked by the DSP of the optical coherent transceiver being the phase and the SOP [3]:

Phase Modulation: The acoustic strain alters both the fibre's physical length (L) and its refractive index (n) via the elasto-optic effect [6]. This directly modulates the accumulated phase (ϕ) of the light, as given by:

$$\Delta\phi = \frac{2\pi}{\lambda_0}\Delta(nL) \tag{1}$$

where λ_0 is the vacuum wavelength [6]. This phase modulation is the primary information carrier in many interferometric sensors.

Polarisation Modulation: Mechanical stress also induces local, time-varying birefringence (B) in the fibre [7], where B is given by:

$$B = |n_x - n_y| \tag{2}$$

where n_x and n_y are the x and y axis refractive indices [7]. This causes the two orthogonal polarisation modes to travel at different velocities, accumulating a differential phase shift (retardance) that changes the light's overall SOP [8]. The change in SOP is therefore an indicator of the acoustic perturbation.

2.2 Data Extraction from a Coherent Transceiver

Polarisation tracking is performed by the transceiver's adaptive 2×2 Multiple-Input Multiple-Output (MIMO) equaliser. The equaliser's filter tap coefficients, updated via the Constant Modulus Algorithm (CMA), are contained in four vectors, $\mathbf{w}_{ab}$, where the subscripts $a, b \in \{H, V\}$ denote the polarisation components. These filter taps converge to represent the inverse of the fibre's Jones matrix [9]. The equalised fields, y_H and y_V, are recovered from the received fields, x_H and x_V, through the convolution operation described by:

$$\begin{bmatrix} y_H(n) \\ y_V(n) \end{bmatrix} = \begin{bmatrix} \mathbf{w}_{HH}^T & \mathbf{w}_{VH}^T \\ \mathbf{w}_{HV}^T & \mathbf{w}_{VV}^T \end{bmatrix} \begin{bmatrix} \mathbf{x}_H(n) \\ \mathbf{x}_V(n) \end{bmatrix} \tag{3}$$

where n is the discrete time index, and $\mathbf{x}_H(n)$ and $\mathbf{x}_V(n)$ are vectors containing the present and past samples of the input signals.

To analyse the slowly-varying polarisation effects, we consider the frequency response of these filters, given by the Discrete-Time Fourier Transform, $W_{ab}(\omega)$. The DC component of this response, $W_{ab}(0)$, is used to determine the SOP. The coefficients used for this calculation, $W_{HH}(0)$ and $W_{VH}(0)$, correspond to the top row of the inverse Jones matrix. They describe the SOP of the signal component at the receiver that was originally launched in the horizontal polarisation. The normalised Stokes parameters (s_1, s_2, s_3) are calculated as follows [3]:

$$s_1 = \frac{|W_{HH}(0)|^2 - |W_{VH}(0)|^2}{S_0} \tag{4}$$

$$s_2 = \frac{2|W_{HH}(0)||W_{VH}(0)|\cos(\Delta\phi)}{S_0} \tag{5}$$

$$s_3 = \frac{2|W_{HH}(0)||W_{VH}(0)|\sin(\Delta\phi)}{S_0} \tag{6}$$

where the total power is given by $S_0 = |W_{HH}(0)|^2 + |W_{VH}(0)|^2$ and the relative phase is $\Delta\phi = \arg(W_{HH}(0)W_{VH}^*(0))$ [10]. Tracking these parameters allows one to observe SOP variation caused by acoustic waves.

Carrier Phase: Following polarisation equalisation, a principal component analysis-based carrier phase estimation block compensates for phase drifts [2]. The output of this stage provides a direct measurement of the carrier phase variations, including those induced by acoustic signals.

By logging these two data streams, the coherent transceiver, designed for communication, is effectively repurposed as a dual-channel acoustic sensor.

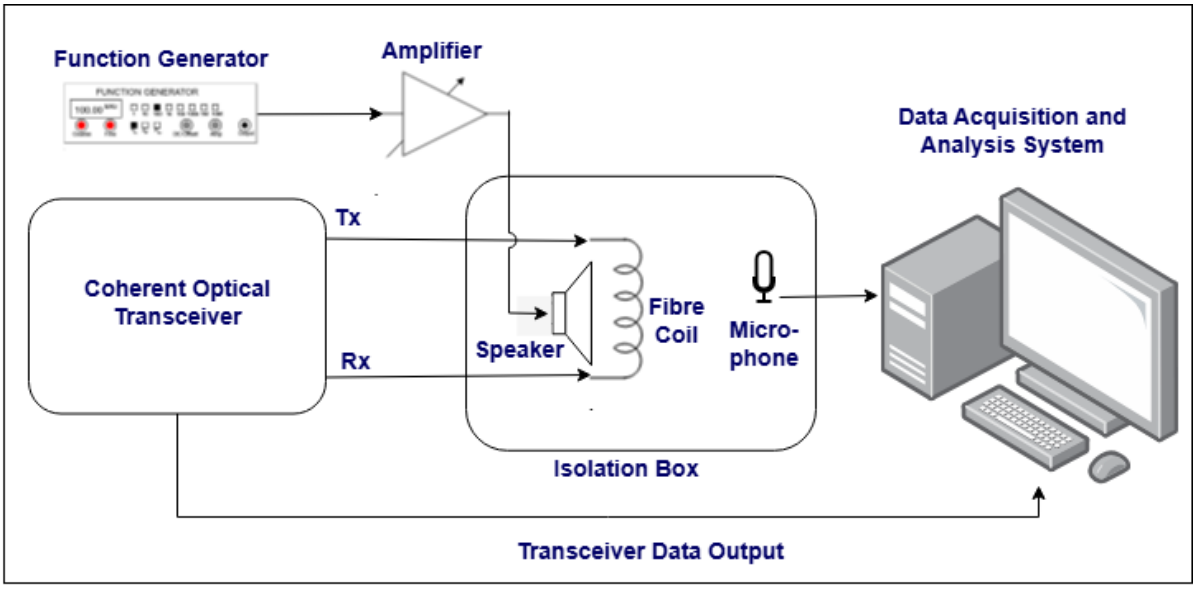

Figure 1: Diagram of the Experimental Setup

3 Experimental Setup and Methodology

The experimental setup, shown schematically in Figure 1, is designed to measure the response of a coherent optical link to airborne acoustic signals in a controlled environment. The system's core is a coherent optical transceiver platform, which allows for real-time extraction of SOP and carrier phase data from its DSP pipeline.

The FPGA-based transceiver employs a 15 kHz-linewidth laser operating at 1550 nm and manages the modulation and signal reception at 2 GS/s. Within the DSP, the two key data sources for sensing are SOP information, derived from the coefficients of a 17-tap per-branch 2x2 MIMO adaptive equaliser updated via the CMA algorithm, and phase information, extracted from a principal component-based carrier phase estimation block using 64-symbol block averaging. The update rates and processing parameters (e.g., CMA step-size, block averaging) of these DSP stages fundamentally define the achievable sensing bandwidth. For the experiments presented, the final logged data rate for both SOP and phase parameters was limited to 15.2 kS/s due to data streaming and storage constraints. Recorded data was analysed in Python and MATLAB, primarily in the frequency domain. Spectrograms and Power Spectral Density (PSD) plots were used to observe the temporal evolution and relative power of the detected frequency components for each signal type. These analyses enabled qualitative evaluation of the system's ability to detect and resolve the applied acoustic stimuli.

The sensing medium is a 1-metre segment of standard OS2 single-mode fibre, housed within a custom-built, acoustically isolated enclosure lined with dense foam to minimise external noise. The majority of the fibre is taped to the enclosure's base, leaving a 10 cm segment untaped and free to interact with the sound field. An external function generator and amplifier drive a speaker positioned 5 cm away from this untaped fibre segment. To precisely quantify the acoustic stimulus, a microphone is placed adjacent to the fibre, also 5 cm from the speaker, ensuring that the Sound Pressure Level (SPL) it records accurately represents the acoustic pressure at the fibre. The resulting SOP and phase data streams are sent to a logging computer via an ethernet cable.

To evaluate the system's acoustic sensing performance, three types of acoustic signals were generated, played through the speaker and directed at the untaped fibre segment: First, a pure 3 kHz sine wave was played, producing an SPL of approximately 112 dB at the fibre. This served as a baseline test to confirm that the system could reliably detect a continuous tone in both SOP and phase data streams. To characterise the system's response across a wider frequency range, both linear and sinusoidal sweeps were performed, covering 20 Hz to 4 kHz. This experiment aimed to observe the frequency-dependent sensitivity and to identify any resonant peaks or nulls in the system's response. The input SPL varied with frequency due to the speaker's inherent frequency response. Finally, a segment of broadband audio (music) was played to qualitatively assess the system's ability to resolve a complex, non-stationary signal with multiple, simultaneous, and time-varying frequency components.

4 Results

The results from the three experiments demonstrate the system's ability to detect and resolve various acoustic signals via SOP and carrier phase measurements. This section presents representative spectrograms and PSD plots for each experiment, highlighting key observations.

4.1 Experiment 1: Single-Frequency Tone

Figure 2 shows the spectrograms of the SOP and carrier phase data streams when subjected to a 3 kHz continuous tone at the fibre. Both channels exhibit a distinct spectral line at 3 kHz, confirming successful detection. The carrier phase data additionally reveals harmonics at 6 kHz, which are absent in the SOP data, indicating different channel characteristics. Furthermore, the phase data shows a lower noise floor, evident from the stronger contrast between signal and background.

Figure 3 presents the corresponding PSDs for SOP and carrier phase, reinforcing these findings by showing a clear peak at 3 kHz in both cases, with a significant secondary peak at 6 Khz showing in the phase data. To quantify the difference in noise between the two channels, the Signal-to-Noise Ratio (SNR) was estimated from the PSD by comparing the integrated power within the signal's frequency band to the power within an adjacent, equivalent-width noise band. The SNR for the S3 parameter (which exhibited the highest SNR of the three Stokes parameters) was 4.65dB, in contrast to the carrier phase SNR of 18.17dB.

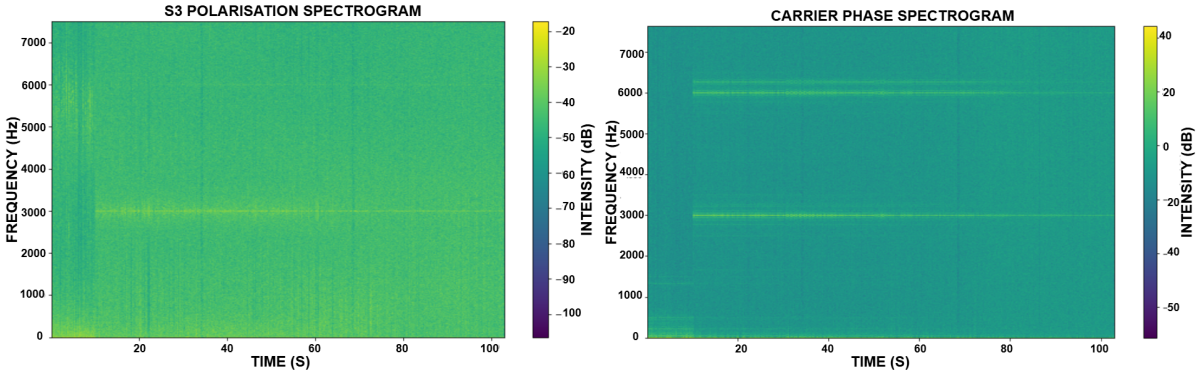

Figure 2: Spectrograms of (*left*) SOP and (*right*) carrier phase data streams during 3 kHz tone excitation. Both show clear detection of the fundamental frequency, while the phase data additionally exhibits harmonics.

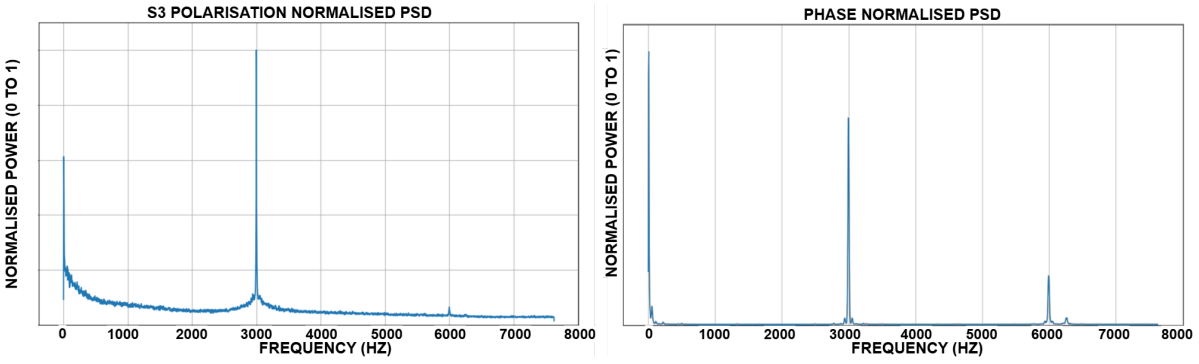

Figure 3: PSD plots of (*left*) SOP and (*right*) carrier phase data during 3 kHz tone excitation, showing strong peaks at the excitation frequency.

4.2 Experiment 2: Frequency Sweeps

Figure 4 shows spectrograms of SOP and phase data for both linear and sinusoidal acoustic frequency sweeps. In all cases, the detected signal closely follows the applied sweep, demonstrating consistent system response over the full frequency range. Harmonics are observed in both polarisation and phase channels.

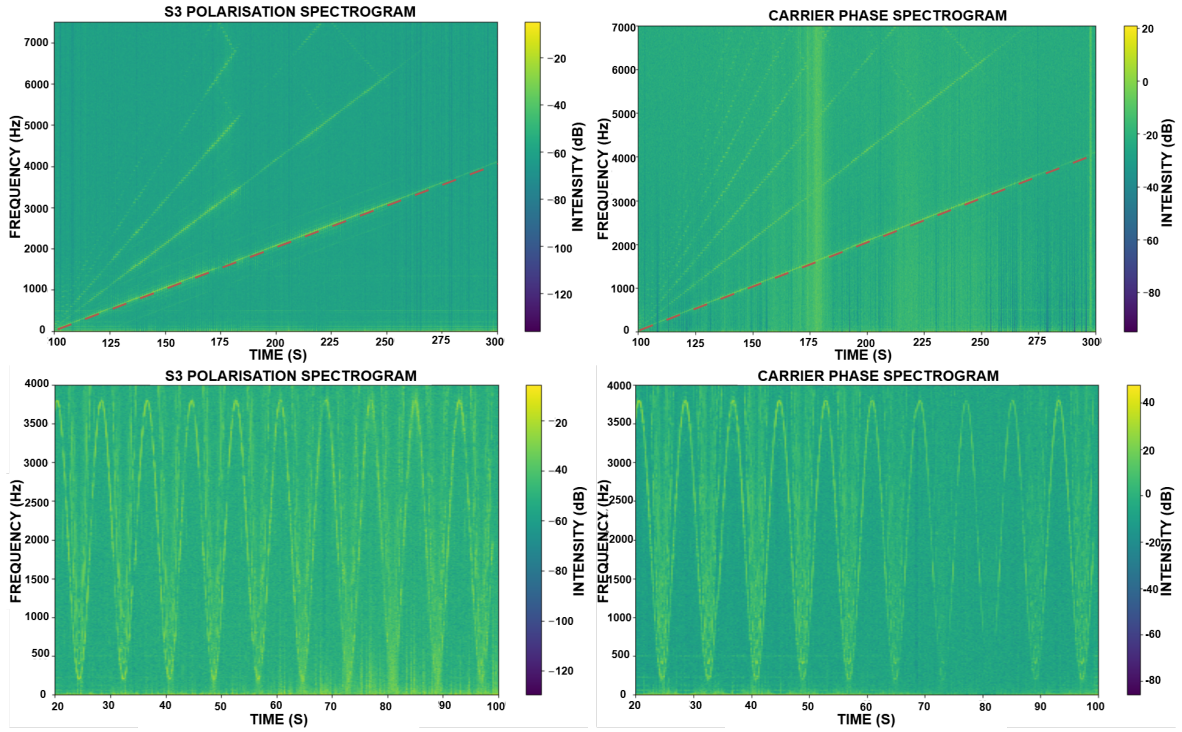

Figure 4: Spectrograms of SOP (*left*) and carrier phase (*right*) data during (*top row*) linear and (*bottom row*) sinusoidal frequency sweeps. Both channels follow the sweep (*red line*) consistently and exhibit additional harmonics.

4.3 Experiment 3: Broadband Audio Signal

For the broadband audio test, the signal was reconstructed from the SOP and phase channels, both of which exhibited strong similarity to the original audio. Only the SOP spectrogram is shown in Figure 5 for brevity. The detected SOP spectrogram closely matches the original, demonstrating the system's ability to resolve complex signals with multiple simultaneous frequency components.

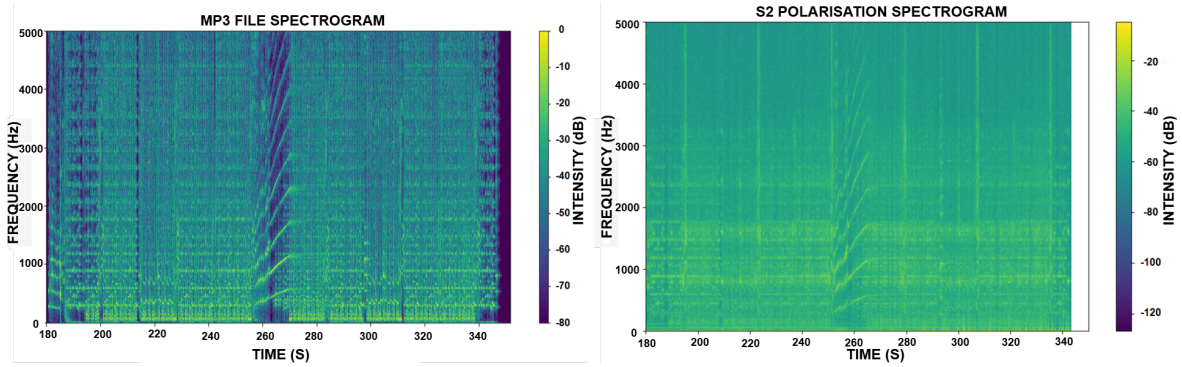

Figure 5: Spectrograms of (*left*) original broadband audio signal and (*right*) SOP data reconstructed signal. The strong correspondence demonstrates the system's ability to resolve complex acoustic signals.

5 Discussion

These preliminary results demonstrate that both the SOP and phase data extracted from a coherent transceiver are capable of detecting and reconstructing complex, broadband acoustic signals, thereby validating the core concept of this sensing approach. In addition, the distinct characteristics exhibited by the polarisation and phase channels

highlight the potential for advanced sensor-fusion techniques. While these findings establish proof of concept, a comprehensive characterisation of the system's minimum detectable SPL, bandwidth and noise floor remains outstanding. This systematic evaluation will constitute the primary focus of future work, which will also include a quantitative comparison of polarisation and phase channels across different deployment scenarios such as overhead lines, underground conduits and subsea cables. Additionally, future work will explore sensor-fusion strategies that combine polarisation and phase information, possibly augmented by machine-learning algorithms, to enhance signal-to-noise ratio and detection accuracy. Ultimately, this research aims to lay the groundwork for transforming existing global telecommunication networks into a dual-purpose network for both communication and acoustic sensing.

6 Conclusion

This work demonstrates the use of SOP and phase data from coherent transceivers for acoustic sensing. Future work will quantify system performance, compare SOP and phase sensing channels, evaluate deployment scenarios, and examine sensor fusion techniques to improve detection capability.

References

[1] E. Ip, F. Ravet, H. Martins, M.-F. Huang, T. Okamoto, S. Han, C. Narisetty, J. Fang, Y.-K. Huang, M. Salemi, E. Rochat, F. Briffod, A. Goy, M. del Rosario Fernández-Ruiz, and M. G. Herráez, "Using Global Existing Fiber Networks for Environmental Sensing," *Proceedings of the IEEE*, vol. 110, no. 11, pp. 1853–1888, Nov. 2022, conference Name: Proceedings of the IEEE. [Online]. Available: https://ieeexplore.ieee.org/document/9881563

[2] M. Mazur, J. C. Castellanos, R. Ryf, E. Börjeson, T. Chodkiewicz, V. Kamalov, S. Yin, N. K. Fontaine, H. Chen, L. Dallachiesa, S. Corteselli, P. Copping, J. Gripp, A. Mortelette, B. Kowalski, R. Dellinger, D. T. Neilson, and P. Larsson-Edefors, "Transoceanic Phase and Polarization Fiber Sensing using Real-Time Coherent Transceiver," in *2022 Optical Fiber Communications Conference and Exhibition (OFC)*, 2022, pp. 1–3.

[3] Z. Zhan, M. Cantono, V. Kamalov, A. Mecozzi, R. Müller, S. Yin, and J. C. Castellanos, "Optical polarization–based seismic and water wave sensing on transoceanic cables," *Science*, vol. 371, no. 6532, pp. 931–936, 2021, _eprint: https://www.science.org/doi/pdf/10.1126/science.abe6648. [Online]. Available: https://www.science.org/doi/abs/10.1126/science.abe6648

[4] M. Mazur, L. Dallachiesa, R. Ryf, D. Wallberg, E. Börjesson, M. Bergroth, B. Josefsson, N. K. Fontaine, H. Chen, D. T. Neilson, J. Schröder, P. Larsson-Edefors, and M. Karlsson, "Real-Time Monitoring of Cable Break in a Live Fiber Network using a Coherent Transceiver Prototype," 2023, _eprint: 2307.01291. [Online]. Available: https://arxiv.org/abs/2307.01291

[5] I. Abu-Mahfouz, "Vibration and Sound Measurements," in *Instrumentation:Theory and Practice Part II: Sensors and Transducers*, I. Abu-Mahfouz, Ed. Cham: Springer International Publishing, 2022, pp. 51–76. [Online]. Available: https://doi.org/10.1007/978-3-031-79211-3_4

[6] L. Kruger and H. J. Theron, "Optical fibre Mach-Zehnder Microphone," in *2007 SBMO/IEEE MTT-S International Microwave and Optoelectronics Conference*, Oct. 2007, pp. 389–391. [Online]. Available: https://ieeexplore.ieee.org/abstract/document/4404287

[7] A. K. Ghatak and K. Thyagarajan, *An Introduction to Fiber Optics*. Cambridge University Press, Jun. 1998.

[8] J. S. Baba, B. D. Cameron, and G. L. Cote, "Effect of temperature, pH, and corneal birefringence on polarimetric glucose monitoring in the eye," *Journal of Biomedical Optics*, vol. 7, no. 3, pp. 321–328, Jul. 2002, publisher: SPIE. [Online]. Available: https://www.spiedigitallibrary.org/journals/journal-of-biomedical-optics/volume-7/issue-3/0000/Effect-of-temperature-pH-and-corneal-birefringence-on-polarimetric-glucose/10.1117/1.1484163.full

[9] M. S. Faruk and S. J. Savory, "Digital Signal Processing for Coherent Transceivers Employing Multilevel Formats," *Journal of Lightwave Technology*, vol. 35, no. 5, pp. 1125–1141, 2017.

[10] E. Collett, *Field guide to polarization*. SPIE press Bellingham, 2005, vol. 15.